Available online at www.sciencedirect.com
SCIENCE DIRECT®
Pergamon
Acta Materialia 51 (2003) 1–15
Acta MATERIALIA
www.actamat-journals.com

Discrete dislocation plasticity modeling of short cracks in single crystals

V.S. Deshpande [a], A. Needleman [b,*], E. Van der Giessen [c]

[a] *Cambridge University, Department of Engineering, Trumpington Street, Cambridge CB2 1PZ, UK*
[b] *Brown University, Division of Engineering, Providence, RI 02912, USA*
[c] *University of Groningen, Department of Applied Physics, Nyenborgh 4, 9747 AG Groningen, The Netherlands*

Received 26 June 2002; accepted 27 August 2002

Abstract

The mode-I crack growth behavior of geometrically similar edge-cracked single crystal specimens of varying size subject to both monotonic and cyclic axial loading is analyzed using discrete dislocation dynamics. Plastic deformation is modeled through the motion of edge dislocations in an elastic solid with the lattice resistance to dislocation motion, dislocation nucleation, dislocation interaction with obstacles and dislocation annihilation incorporated through a set of constitutive rules. The fracture properties are specified through an irreversible cohesive relation. Under monotonic loading conditions, with the applied stress below the yield strength of the uncracked specimen, the initiation of crack growth is found to be governed by the mode-I stress intensity factor, calculated from the applied stress, with the value of K_{init} decreasing slightly with crack size due to the reduction in shielding associated with dislocations near a free surface. Under cyclic loading, the fatigue threshold is ΔK-governed for sufficiently long cracks. Below a critical crack size the value of ΔK_{I} at the fatigue threshold is found to decrease substantially with crack size and progressive cyclic crack growth occurs even when $K_{\max}$ is less than that required for the initiation of crack crack growth in an elastic solid. The reduction in the fatigue threshold with crack size is associated with a progressive increase in internal stress under cyclic loading. However, for sufficiently small cracks, the dislocation structure generated is sparse and the internal stresses and plastic dissipation associated with this structure alone are not sufficient to drive fatigue crack growth.

Keywords: Dislocations; Mechanical properties; Fatigue, plastic; Computer simulation; Short cracks

1. Introduction

Short fatigue cracks in metallic components grow faster than long cracks subject to the same applied stress intensity factor range. This phenomenon, which has been long recognized, see [1,2] for reviews of the relevant literature, is a critical issue for the fatigue resistant design of a broad range of structures and components. Neglecting the enhanced growth rate of short cracks can result in a substantial overestimate of the fatigue life.

Suresh and Ritchie [1] (also see [3]) have introduced a classification scheme to distinguish the ori-

* Corresponding author. Tel.: +1-401-863-2863; fax: +1-401-863-1157.
E-mail address: needle@engin.brown.edu (A. Needleman).

1359-6454/03/$22.00
doi:10.1016/S1359-6454(02)00401-9

gin of the size effect: (i) microstructurally small cracks, e.g. cracks comparable in length to the grain size in a polycrystal; (ii) mechanically small cracks, e.g. a crack tip plastic zone size comparable to the crack length; (iii) physically small cracks, a crack length on the order of millimeters; and (iv) chemically small cracks, where a size effect arises from environmental factors such as stress corrosion fatigue.

For sufficiently long cracks, the fatigue threshold ΔK_{th} is independent of crack length. However, Kitagawa and Takahashi [4] showed that, for a wide variety of ductile metals, there is a critical crack length below which ΔK_{th} decreases with decreasing crack length and the fatigue limit is characterized by a critical stress range $\Delta\sigma_{th}$ for sufficiently small cracks. Although there is a large experimental literature documenting this phenomenon for polycrystalline metals [4] and for single crystals [5,6], there is very little understanding of the mechanisms which cause this reduction in the fatigue threshold.

A continuum plasticity model to account for this short crack effect in polycrystals was proposed by Tanaka et al. [7]. It presumes that a slip band emanating from the crack tip is blocked by a grain boundary. Other grain boundary blocking models have also been analyzed, see for example Wang and Hutchinson [8]. While such models qualitatively predict some experimental observations such as the enhanced resistance to crack initiation with decreasing grain size, they do not pertain to single crystals which exhibit the same sort of crack size dependence of the fatigue threshold as do polycrystals.

Several models have been proposed that can be applied to single crystals. Usami and Shida [9] postulated that the fatigue threshold corresponds to a critical size of the cyclic plastic zone for all crack sizes. Using the Dugdale plastic zone estimate they showed that this hypothesis qualitatively predicts the variation of the fatigue threshold with crack length. However, the authors provided no physical basis for their hypothesis. Caracostas et al. [10] analyzed the behavior of mode-III edge cracks via a double slip plane crack model. They calculated the dislocation density distribution on the two slip planes parallel to the crack and inferred crack growth rates from the slip rates. This model predicted reductions in both the monotonic and cyclic crack growth resistances with decreasing crack length due to the reduced shielding associated with screw dislocations near a free surface. The models in Refs. [9,10] predict a deviation from *K*-governed behavior only when the applied stress is approximately equal to the yield strength of the material; experiments suggest that fatigue crack growth is enhanced for short cracks in edge-cracked specimens even when the maximum applied stress is as low as a third of the yield strength [11].

Nguyen et al. [12] carried out numerical calculations of fatigue crack growth in which the material was characterized by a conventional continuum plasticity model and the fracture properties were embedded in a cohesive relation with loading-reloading hysteresis and cyclic softening. They find accelerated fatigue crack growth rates when the crack length is of the order of the cohesive length (the length scale over which large stress gradients occur ahead of the crack in an elastic solid). Recently, Vasudevan et al. [13] suggested that a progressive increase in internal stresses under cyclic loading provides an additional driving force for short cracks which results in a reduction in the measured macroscopic fatigue threshold, but no quantitative calculations were carried out.

Here we present analyses for single crystals carried out within a purely mechanical framework, so that any size effects are mechanical or physical according to the classification scheme of Suresh and Ritchie [1]. The framework is the same as used to analyze the near-threshold [14] and Paris law regimes [15] for long cracks. A key feature of the formulation is that the material model and the fracture properties are independent of the crack size and the mode of loading. Indeed, the material model is also applicable when there is no crack, as, for example, in Ref. [16]. The material is a planar model crystal with three slip systems with plastic flow arising from the collective motion of large numbers of edge dislocations, which are represented as line singularities in an elastic solid. The long-range interactions between dislocations and with free surfaces are directly accounted for. Drag during dislocation motion, interactions with obstacles, and dislocation nucleation and annihil-

ation are incorporated through a set of constitutive rules. The fracture properties are embedded in a cohesive surface constitutive relation so that crack initiation and crack growth emerge as natural outcomes of the simulation.

A plane-strain boundary value problem is formulated and solved for a 90° edge-cracked specimen subject to monotonic or cyclic tensile loading. Geometrically similar specimens having a range of crack lengths are analyzed. For sufficiently large specimens, small scale yielding conditions prevail, as assumed from the outset in [14,15]. On the other hand, for sufficiently small specimens, the near-tip plastic zone size becomes comparable to the crack length and the cracks are *mechanically* short cracks as defined in [1,2]. Our main focus here is on the crack size dependence of the fatigue threshold.

2. Discrete dislocation formulation

The framework used is one where full boundary value problem solutions are obtained with plastic flow arising from the collective motion of a large number of dislocations. The particular problem considered is a planar single crystal with an edge crack subject to either monotonic or cyclic uniaxial loading. Plane strain analyses are carried out with the crystal taken to have three slip systems, with each slip plane at an angle $\phi^{(\alpha)}$, $\alpha = 1, 2, 3$, from the tensile axis as shown in Fig. 1a. In all calculations, $\phi^{(1)} = -\phi^{(2)} = 35.3°$ and $\phi^{(3)} = 90°$.

The boundary value problem formulation is that of Van der Giessen and Needleman [17] and has been used to solve a variety of boundary value problems including, for example, bending of a planar strip [16], monotonic [18] and cyclic loading [14,15] of a crack in small scale yielding and thermal stress development in thin films [19]. The formulation is an incremental one where at any time t, the body is in equilibrium with the applied loads and displacements, and the position of each dislocation in the body is known. An increment of loading is applied and the stress and displacement fields, and the dislocation structure are determined at $t+\Delta t$.

The dislocations are treated as line singularities in an elastic continuum, with the crystal taken to be elastically isotropic with shear modulus $G = 26.3$ GPa and Poisson's ratio $\nu = 0.33$, which are representative values for aluminum. Consistent with the plane strain condition, only edge dislocations are considered, all having the same Burgers vector, $b = 0.25$ nm. The potentially active slip planes are spaced at $90b$.

The long range elastic interactions between dislocations are accounted for directly in the boundary value problem solution. Short range interactions enter through a set of constitutive rules of the type suggested by Kubin et al. [20]. Constitutive rules are specified for: (i) dislocation glide; (ii) annihilation; (iii) nucleation; (iv) obstacle pinning. The glide velocity is taken to be linearly related to the Peach-Koehler force with a drag coefficient $B = 10^{-4}$ Pa s, a representative value for several fcc crystals [20]. Dislocations of opposite sign annihilate when they come within a critical distance of $L_e = 6b$. Initially, the three slip systems are free of mobile dislocations, but dislocations can be generated from discrete sources that are randomly distributed with a density of $64/\mu m^2$. These point sources mimic Frank-Read sources from pinned segments on out-of-plane slip systems which are not explicitly considered. They generate a dipole when the Peach-Koehler force exceeds a critical value of $\tau_{nuc}b$ during a period of time t_{nuc}; here $\tau_{nuc} = 50$ MPa and $t_{nuc} = 10$ ns. There is also a random distribution of 148 point obstacles per μm^2, which represent either small precipitates on the slip plane or forest dislocations on out-of-plane slip systems. The obstacles pin dislocations as long as the Peach-Koehler force is below the obstacle strength $b\tau_{obs}$, where $\tau_{obs} = 150$ MPa. The source and obstacle distributions over a representative $2\ \mu m \times 2\ \mu m$ region are shown in Fig. 1b.

At each time step, the stress and displacement fields are obtained by superposition as described in [17]. The fields are written as

$$\sigma_{ij} = \tilde{\sigma}_{ij} + \hat{\sigma}_{ij}, \qquad u_i = \tilde{u}_i + \hat{u}_i, \tag{1}$$

where the $(\tilde{})$-fields are the singular fields associated with each individual dislocation, e.g.,

$$\tilde{\sigma}_{ij} = \sum_{I=1}^{N} \tilde{\sigma}_{ij}^{(I)}$$

where N is the number of dislocations and $\tilde{\sigma}_{ij}^{(I)}$ is

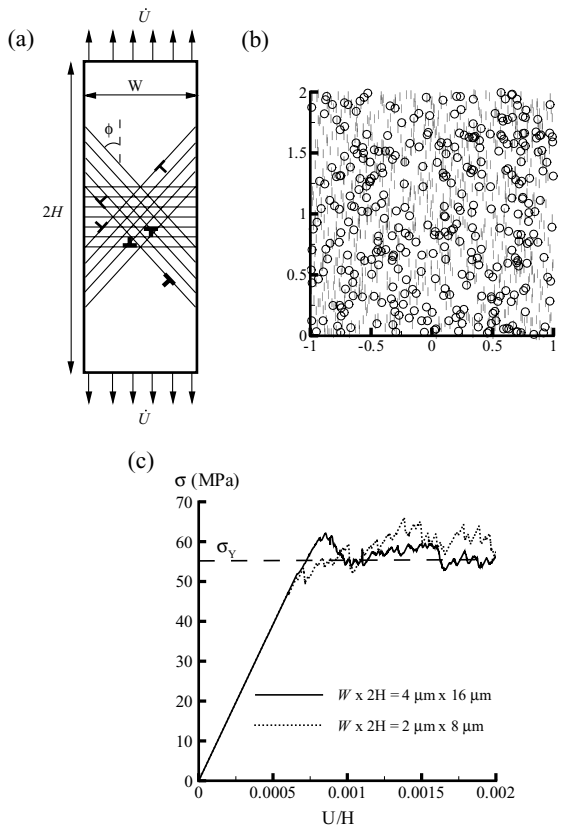

Fig. 1. (a) Sketch of the boundary value problem analyzed to obtain the uniaxial stress versus strain response of the uncracked single crystal. (b) Dislocation source and obstacle distribution in a $2\ \mu m \times 2\ \mu m$ region for the material with $\rho_{nuc} = 64/\mu m^2$ and $\rho_{obs} = 148/\mu m^2$. The dislocation sources are represented by "o" and the obstacles by "|". (c) The uniaxial tensile stress versus strain (U/H) response of the material for two geometrically similar specimens.

the stress field associated with dislocation I in the half-space $x_2 \geq 0$. The $(\hat{})$-fields are image fields that enforce the boundary conditions. The $(\hat{})$-fields are smooth and are obtained by a finite element method.

For comparison purposes, results will be presented for the uncracked tensile bar shown in Fig. 1a. The origin of the coordinate system is placed where the mid-plane meets the free surface so that the bar occupies $0 \leq x_1 \leq W$ and $-H \leq x_2 \leq H$. With symmetry about the origin assumed, the region $x_2 \geq 0$ is analyzed. A displacement rate $\dot{U}$ and shear free conditions are prescribed on the edge where the loading is imposed,

$$\dot{u}_2 = \dot{U},\ \dot{T}_1 = 0 \quad \text{on } x_2 = H. \tag{2}$$

Here, $(\dot{})$ denotes time differentiation and the traction $T_i = \sigma_{ij} n_j$, where n_j is the outward normal to the appropriate surface.

The lateral sides are traction free

$$\dot{T}_1 = \dot{T}_2 = 0 \quad \text{on } x_1 = 0, W, \tag{3}$$

and symmetry conditions on the center-line are given by

$$\dot{u}_2 = 0,\ \dot{T}_1 = 0 \quad \text{on } x_2 = 0. \tag{4}$$

The predicted stress versus strain response is shown in Fig. 1c for two uncracked specimens, one having dimensions half the other, with the prescribed loading rate being $\dot{U}/H = 100/\text{s}$. The stress σ is computed as

$$\sigma = \frac{1}{W}\int_0^W T_2(x_1, H)\,dx_1. \tag{5}$$

There is no significant difference between the stress versus strain curves of the two specimens. In both cases, the stress versus strain behavior is linear up to a yield strength of $\sigma_Y \approx 55$MPa, which is slightly greater than the dislocation nucleation stress, τ_{nuc}, and then the overall behavior is essentially ideally plastic with the fluctuations a result of the relatively small volume over which the discrete dislocation activity is averaged.

The boundary value problem for the edge-cracked specimen is identical to that for the uncracked specimen except that the symmetry boundary condition (4) is replaced by a traction free condition along a crack of length a

$$\dot{T}_1 = \dot{T}_2 = 0 \quad \text{on } x_2 = 0 \text{ and } x_1 < a \tag{6}$$

together with a cohesive surface ahead of the crack for $a \leq x_1 \leq W$. In addition, for computational convenience, dislocation activity is restricted to a process window of dimensions $L_p \times h_p$: h_p is always taken to be 50 μm; L_p is 25 μm on either side of the initial crack tip (50 μm total) unless $a <$ 25 μm in which case $L_p = a + 25\ \mu m$. Computations are terminated before any dislocations reach

the boundary of the process window so that the effect of the process window is to restrict the loading range that can be analyzed. The boundary value problem analyzed numerically is sketched in Fig. 2a. Note that dislocations are allowed to exit into the open crack and from the face $x_1 = 0$ if the process window extends to that edge. Results will be presented for geometrically similar specimens with $H = 12.5\ W$ and $a/W = 0.1$, having various sizes (identified here through the crack length a).

Along the cohesive surface $T_1 = 0$ (from symmetry) while T_2 has the universal binding form [21],

$$T_2(\Delta_2) = -e\sigma_{\mathrm{coh}}\frac{\Delta_2}{\delta_{\mathrm{n}}}\exp\left(-\frac{\Delta_2}{\delta_{\mathrm{n}}}\right), \tag{7}$$

where $\Delta_2 = 2u_2(x_1,0)$, σ_{coh} is the normal cohesive strength and δ_n is a characteristic length.

For monotonic separation, the work of separation is given by $\phi_n = \exp(1)\sigma_{\mathrm{coh}}\delta_n$ and is related to a reference stress intensity factor K_0 by

$$K_0 = \sqrt{\frac{E\phi_n}{1-\nu^2}}, \tag{8}$$

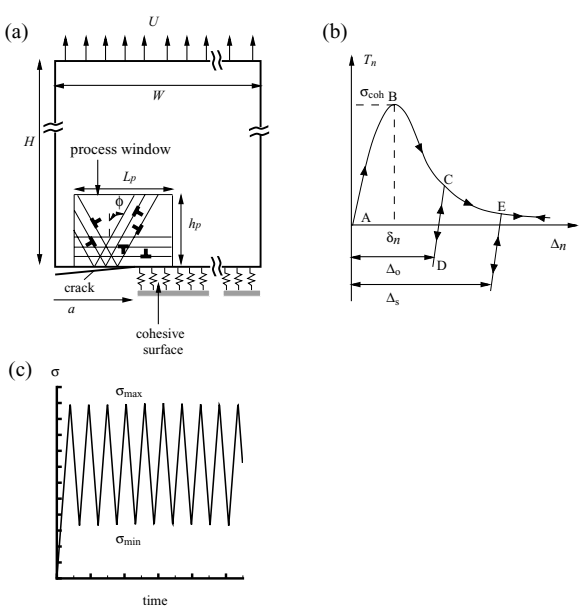

Fig. 2. (a) 90° edge crack problem with the imposed boundary conditions. (b) Schematic of the cohesive relation employed. (c) Schematic of the applied stress as a function of time.

with $E = 2(1 + \nu)G$. The significance of K_0 is that pure mode-I crack growth in a homogeneous elastic solid with the given cohesive properties takes place at $K_I/K_0 = 1$ [22]. Unless otherwise specified the cohesive properties were taken as $\sigma_{\mathrm{coh}} =$ 0.75 GPa and $\delta_n = 2b$ giving a work of fracture $\phi_n \approx 1.0\ \mathrm{J/m^2}$ and $K_0 \approx 0.280\ \mathrm{MPa}\sqrt{\mathrm{m}}$.

The effect of the formation of an oxide layer and the subsequent surface contact during unloading is modeled by specifying unloading from and reloading to the monotonic cohesive law as illustrated in Fig. 2b. The relation (7) describes the loading response as the traction increases from A up to the maximum value at B, followed by softening while the formed crack opens further. Unloading from any point C takes place along path CD, with stiffness

$$\frac{\partial T_2}{\partial \Delta_2} = -\frac{\exp(1)\sigma_{\mathrm{coh}}}{\delta_n}. \tag{9}$$

On reloading the traction increases along DC and then follows the original softening curve BCE. Under continued cyclic loading conditions, the permanent opening Δ_o (see Fig. 2b) grows, but not more than a specified value of Δ_s. This represents the asymptotic value of the oxide layer thickness formed on a metal surface: under ambient conditions this is reported to be 2–6 nm for aluminum [23] and in the calculations we take $\Delta_s = 4$ nm. Further details on the irreversible cohesive surface formulation, including a comparison of the fatigue threshold predictions for reversible and irreversible characterizations of the cohesive response, are given in Ref. [14].

Calculations are carried out for the cracked specimen with $U(t)$ specified to be monotonically increasing and with $U(t)$ a cyclic function of time. In all cases a loading rate $\dot{U}/H = 100/\mathrm{s}$ was employed. This relatively high loading rate was chosen to reduce the time required for the computations. In Ref. [24], under monotonic small scale yielding loading conditions, varying the loading rate by two orders of magnitude did not qualitatively change the crack growth behavior, although a strong tendency was found for increased plastic deformation at lower loading rates. Under cyclic loading conditions, σ computed from (5) has the time variation shown in Fig. 2c. Note that the

boundary value problem for the cracked bar reduces to the uncracked crystal in the limit $a \to 0$ and with $\sigma \ll \sigma_{coh}$.

For an isotropic elastic solid the remote mode-I stress intensity factor can be written as, [25]

$$K_I = C\sigma\sqrt{\pi a} \tag{10}$$

where $C = 1.196$ for $a/W = 0.1$. As long as the solid remains linearly elastic, (10) predicts that the initiation of crack growth, $K_{Ic} = K_0$ scales with $\sqrt{a}$. This scaling remains valid for sufficiently large specimens for which plastic deformation is confined to the near crack tip region. This is the small scale yielding limit, analyzed in Refs. [14,15].

3. Monotonic loading behavior

3.1. Stationary cracks

To gain insight into the differences between the stress fields around long and short cracks, we consider the fields around a stationary crack tip of the edge-cracked specimen loaded in tension. To inhibit crack growth, the cohesive properties in the stationary crack calculations are specified as $\sigma_{coh} = 3$GPa and $\delta_n = 10b$. The dislocation distributions at $K_I/(G\sqrt{b}) = 0.65$, where K_I is calculated from (10), are shown in Fig. 3a and b for specimens with crack sizes $a = 10$ μm and $a = 100$ μm, respectively. At the same value of K_I, the dislocation density is higher near the crack tip for the specimen with the shorter crack. However, the crack profiles (shown below the x_1-axis with the displacements magnified by a factor of 20) in both cases are very similar and show that there has been negligible blunting of the crack. This is consistent with the experimental findings of Guiu and Stevens [26] who observed that short surface cracks remain sharp in the presence of extensive plasticity.

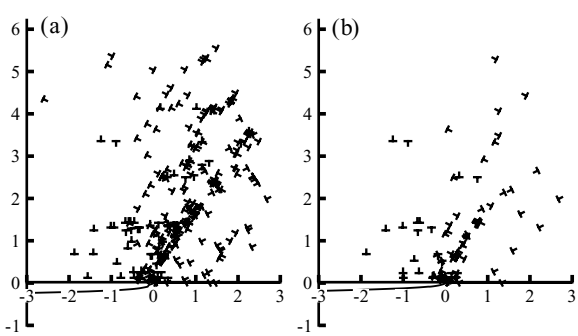

Fig. 3. Dislocation structures around the stationary crack tip at $K_I/(G\sqrt{b}) = 0.65$ for crack lengths (a) $a = 10$ μm and (b) $a = 100$ μm. All distances are in μm. The crack opening profiles (displacements magnified by a factor of 20) are plotted below the x_1-axis.

Distributions of the normalized crack opening stress σ_{22}/σ_Y are also shown, in Figs 4a and b, for the situations corresponding to Figs 3a and b, respectively. Because of the cohesive surface, there is no crack tip singularity and the crack tip stresses are finite (the opening stress cannot exceed σ_{coh}). The crack opening stresses are approximately the same for both specimen sizes even though there is more plastic flow in the smaller specimen, which tends to relax stresses. Counteracting this, the higher dislocation density in the smaller specimen, $a = 10$ μm, tends to increase the stress magnitude in the vicinity of the crack tip. It is also worth noting that analytical solutions for screw dislocations around the crack tip of a mode-III edge crack show that the shielding associated with dislocations near the tip of short edge cracks is reduced due to the image effects associated with the traction free edge [27].

3.2. Crack growth

Curves of K_I/K_o versus crack extension Δa are shown in Fig. 5a for specimens with crack lengths varying from $a = 10$ μm to $a = 500$ μm. Here and subsequently, the crack location is taken to be the point along the cohesive surface where $\Delta_2 = 4\delta_n$. The monotonic crack growth calculations for the specimens with the 10 and 20 μm cracks were terminated after a crack extension $\Delta a \approx 0.03$ μm as dislocations then reach the upper boundary of the process window. The curves of K_I/K_0 versus crack extension are reasonably independent of crack length for $a \geq 300$ μm suggesting that for the material parameters used, monotonic crack growth is governed by K_I for $a \geq 300$ μm. On the other hand, for crack lengths less than ≈ 100 μm, the value of K_I at a particular crack extension decreases with decreasing crack length. This is

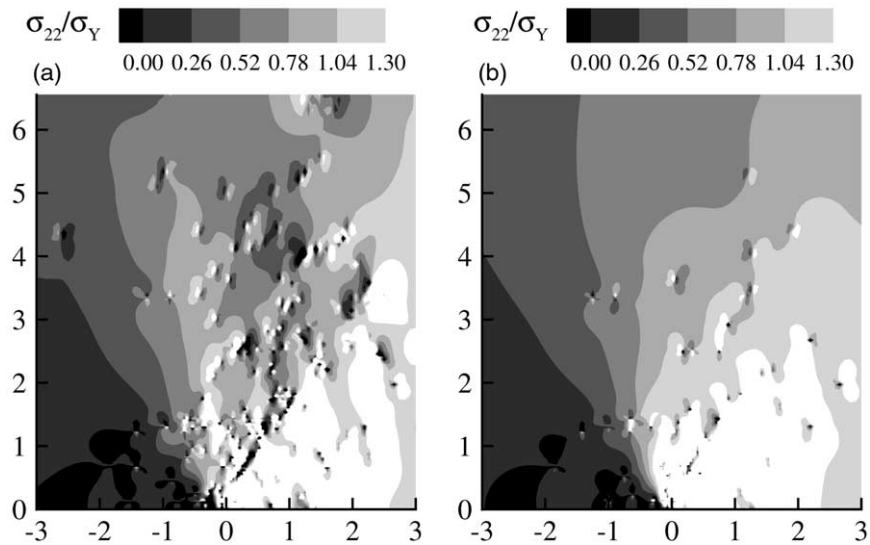

Fig. 4. Distributions of the normalized stress σ_{22}/σ_Y around the stationary crack tip at $K_I/(G\sqrt{b}) = 0.65$ for crack lengths (a) $a = 10$ μm and (b) $a = 100$ μm. All distances are in μm.

seen clearly in Fig. 5b where the mode-I stress intensity factor at the initiation of crack growth, K_{init}, is plotted as a function of crack length: for $a \geq 300$ μm crack growth initiates at $K_I/K_0 \approx 1.32$ with this initiation value decreasing to ≈ 1.15 for $a = 10$ μm. The corresponding value of σ at the initiation of crack growth, σ_{init}, is shown in Fig. 5c as a function of the crack length a. The initiation of crack growth is essentially K-governed for $a > 300$ μm (note the log scale). Figure 5c shows that the value of σ to initiate crack growth in the $a = 10$ μm specimen is approximately equal to the yield strength σ_Y of the uncracked crystal (see Fig. 1c). Calculations for monotonic crack growth in this specimen were terminated at $\Delta a \approx 0.03$ μm as further loading results in overall yielding.

These discrete dislocation crack growth results can be rationalized in terms of the dual role that dislocations play in the fracture process [18]. Although plastic flow due to the motion of dislocations increases the resistance to crack growth and tends to arrest the crack, the local stress concentration associated with the discrete dislocation structure near the crack tip promotes crack propagation. As the crack size decreases, the net effect of increased dislocation activity and a more dense crack tip dislocation structure is that K_{init} decreases somewhat with crack size.

4. Cyclic loading behavior

In the cyclic loading calculations, σ, defined in (5), is varied between σ_{max} and σ_{min} as shown schematically in Fig. 2c with the load ratio $R = \sigma_{min}/\sigma_{max} = 0.3$ in all calculations. To determine the fatigue threshold, calculations are carried out starting at some $\Delta K_I = C\Delta\sigma\sqrt{\pi a}$ and then reducing ΔK_I until a cycle-by-cycle crack growth rate $da/dN \leq 10^{-3}$μm/cycle is obtained. The fatigue threshold is then defined as the mean of the last two values of ΔK_I. Typically, steps of $\Delta K_I/K_0 = 0.05$ were used.

Crack advance versus time curves are shown in Fig. 6 a for three values of ΔK_I for the $a = 100$ μm specimen. For $\Delta K_I/K_0 = 0.885$, the value of K_{max} is greater than required to initiate crack growth under monotonic loading so a "burst" of crack growth occurs during the first loading cycle. Subsequently, an average cycle-by-cycle crack growth of $da/dN \approx 0.02$ μm/cycle is attained over the six additional cycles computed. For

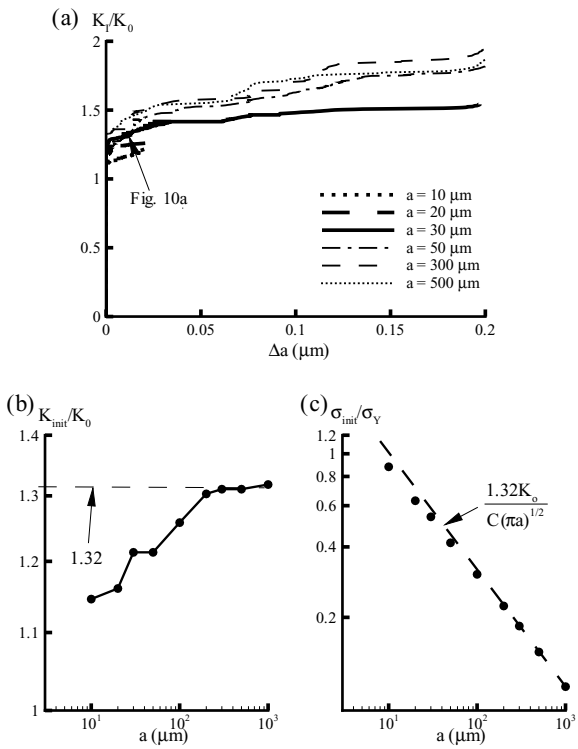

Fig. 5. (a) K_I/K_0 versus crack extension Δa for monotonically loaded geometrically similar specimens with various crack lengths a. (b) Normalized mode-I stress intensity factor at the initiation of crack growth, K_{init}/K_0, as function of crack length a. (c) Normalized applied stress at initiation of crack growth, σ_{init}/σ_Y, as function of crack length a. The dashed lines correspond to K_{init} in the long crack limit.

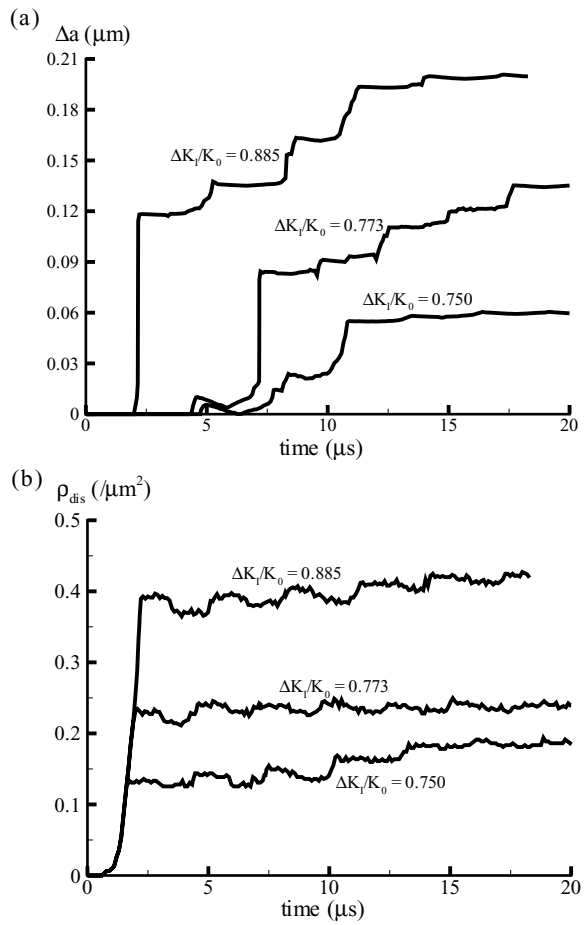

Fig. 6. (a) Time evolution of the crack growth and (b) time evolution of the dislocation density for the edge-cracked specimen with a crack of length a=100 μm at selected values of ΔK_I ($R = 0.3$).

$\Delta K_I/K_0 = 0.773$ and $\Delta K_I/K_0 = 0.750$, crack growth commences during the second loading cycle and subsequently a steady cycle-by-cycle crack growth rate is achieved with $da/dN \approx 10^{-2}$ μm/cycle and $< 10^{-3}$μm/cycle for $\Delta K_I/K_0 =$ 0.773 and 0.750, respectively. Thus, $\Delta K_{th}/K_0 =$ 0.762 for cyclic loading of the $a = 100$ μm specimen ($R = 0.3$). No crack advance was obtained for $\Delta K_I/K_0 < 0.750$.

The evolution of the dislocation density ρ_{dis} (per unit area in the process window) with time is shown in Fig. 6b for the same three values of ΔK_I. For $\Delta K_I/K_0 = 0.885$ the dislocation density increases with the number of loading cycles: the irreversibility of dislocation motion results in an evolving dislocation structure which increases the crack opening stresses and advances the crack at a value of K_{max} at which the crack would have arrested under monotonic loading. On the other hand, for $\Delta K_I/K_0 = 0.773$ and 0.750 the dislocation density increases in the first few cycles followed by nearly no further cycle-by-cycle increase in ρ_{dis}. This is consistent with $0.750 \leq \Delta K_{th}/K_0 \leq$ 0.773.

Similar calculations to probe the fatigue threshold were carried out for geometrically similar specimens with edge crack lengths varying from 10 μm to 1000 μm. Selected curves of crack advance versus time for near-threshold values of ΔK_I are shown in Fig. 7a. No crack advance takes place during the first loading cycle with crack

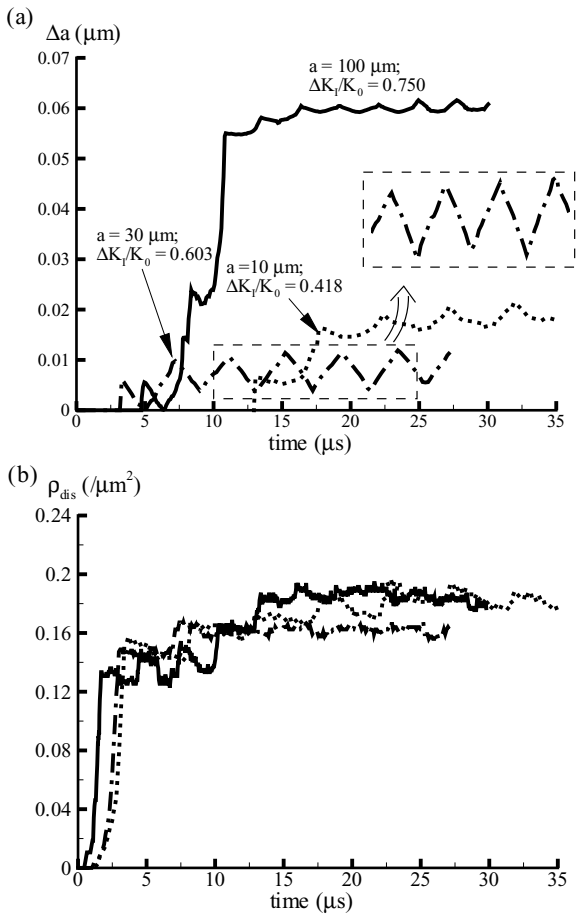

Fig. 7. (a) Time evolution of the crack growth and (b) time evolution of the dislocation density at near-threshold values of applied ΔK_I ($R = 0.3$) for three geometrically similar specimens with different crack lengths a. Note that the dislocation densities are approximately equal for all three specimens.

growth beginning in subsequent cycles due to the build-up of internal stresses associated with the near tip dislocation structure. For the calculations in Fig. 7a, the crack growth rate da/dN settles down to a steady value $\approx 10^{-3}$μm/cycle after the first few cycles. Note that the values of the near-threshold ΔK_I decrease with crack length for these geometrically similar specimens. The evolution of the dislocation densities with time is shown in Fig. 7b. At near-threshold values of ΔK_I, the dislocation density (or the total number of dislocations) is approximately the same in all differently-sized specimens, suggesting that the build-up of internal stresses needed to promote crack advance under cyclic loading is associated with a critical density (or number) of dislocations.

The results of all the fatigue threshold calculations carried out are summarized in Fig. 8a where the normalized fatigue threshold $\Delta K_{th}/K_0$ for the geometrically similar specimens is plotted as a function of the edge crack length, a. Consistent with the monotonic crack growth results, the fatigue threshold ΔK_{th} is approximately independent of crack length for $a \geq 300$ μm. However, ΔK_{th} decreases sharply with crack length below this crack size. In fact, for cracks shorter than

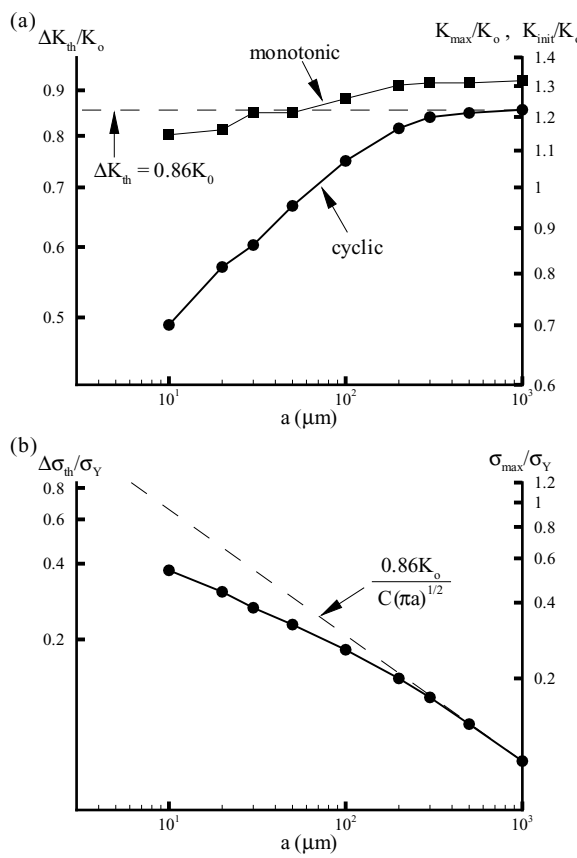

Fig. 8. (a) Normalized fatigue threshold $\Delta K_{th}/K_0$ ($R = 0.3$) versus crack length. For comparison purposes the normalized K_I at the initiation of crack growth under monotonic loading is also shown. (b) The fatigue threshold plotted as the normalized applied stress range $\Delta\sigma_{th}/\sigma_Y$ versus crack length (corresponding values of the maximum applied stress σ_{max}/σ_Y are shown on the right axis).

approximately 100 μm, progressive crack growth takes place for values of $K_{max} < K_0$, where $K_{max} = \Delta K_I/(1-R)$. This indicates that the build-up of internal stresses under cyclic loading results in a net increase in the anti-shielding effect of the dislocations. For comparison purposes the monotonic crack growth results of Fig. 5b are also shown in Fig. 8a; the crack growth enhancement for short cracks is much greater under cyclic loading conditions than for monotonic loading.

The same calculated fatigue thresholds are shown in terms of $\Delta\sigma_{th}$ in Fig. 8b. The $\Delta\sigma_{th}$ versus a curve shows that fatigue is ΔK-governed for $a > 300$ μm. For crack lengths less than 300 μm, the deviation from ΔK-governed fatigue increases with decreasing crack size, with the fatigue threshold for smaller cracks tending to be $\Delta\sigma$ rather than ΔK-governed. Results are shown in Fig. 8 for crack lengths down to only 10 μm; cyclic calculations with $\Delta\sigma = 30$ MPa were carried out for specimens with crack lengths $a = 5$ and 3 μm but crack growth did not initiate in those specimens after the four cycles computed despite the applied stress range being greater than a smooth extrapolation of the data in Fig. 8b.

Fig. 9 shows near crack tip stress contours and dislocations for specimens with crack sizes $a = 10$ μm and $a = 3$ μm. Contours of σ_{22}/σ_Y and the dislocation structure around the crack tip at the first load peak for the specimen with the 10 μm crack is shown in Fig. 9a for the near threshold value $\Delta\sigma_{th}/\sigma_Y \approx 0.4$ ($\sigma_{max}/\sigma_Y \approx 0.57$). Fig. 9b shows a similar plot for the specimen with the 3 μm crack subjected to $\Delta\sigma/\sigma_Y = 0.55$ ($\sigma_{max}/\sigma_Y = 0.79$). In Fig. 9a there is a dense dislocation structure around the crack tip and the stress field differs significantly from an elastic mode-I field. It is this dense dislocation structure that evolves with cyclic loading and generates the anti-shielding effect that initiates crack growth with $K_{max} < K_0$. On the other hand, the dislocation structure around the crack tip of the specimen with the 3 μm crack (Fig. 9b) is sparse because the size of the high stress region at the crack tip decreases with specimen size. For the material parameters used in this study (slip plane spacing, source spacing, source strength, etc.) and for crack sizes of ≈5 μm and smaller, the high stress region near the crack tip is not large enough to nucleate and move many dislocations at values of $\sigma_{max} < \sigma_Y$. Fatigue requires irreversibility[1] and the sparse dislocation structure in Fig. 9b does not induce sufficient irreversibility to give fatigue crack growth: since $K_{max} < K_0$ crack growth is precluded in this essentially elastic crystal.

The predicted plastic deformation patterns are shown in Fig. 10 in terms of distributions of slip which are calculated from the computed displacement field. Although the displacement field is not continuous since dislocation glide gives rise to a displacement jump across the slip plane, the displacements u_i are evaluated on the finite element grid to visualize the deformations and the strain field, $\varepsilon_{ij} = (u_{i,j} + u_{j,i})/2$, is computed by numerical differentiation. A measure of the slip on slip system α, $\gamma^{(\alpha)}$, is then defined by

$$\gamma^{(\alpha)} = s_i^{(\alpha)} \varepsilon_{ij} m_j^{(\alpha)}, \tag{11}$$

where $s_i^{(\alpha)}$ is the tangent and $m_j^{(\alpha)}$ the normal to the slip plane α. The total slip over the three slip systems, $\Gamma = \sum_{\alpha=1}^{3} |\gamma^{(\alpha)}|$, is shown in Fig. 10a and b for monotonic and cyclic loading, respectively of the $a = 30$ μm specimen. In both figures, $\Delta a \approx 0.01$ μm: for monotonic loading this corresponds to $K_I/K_0 \approx 1.3$ as marked in Fig. 5a, while under cyclic loading this corresponds to the third load peak with $K_{max}/K_0 \approx 0.86$. Comparing the two figures it is evident that the increased loading required to propagate the crack under monotonic loading results in an increase in distributed plasticity. Under cyclic loading plastic deformation remains much more localized. Also, note that the extent of significant slip (say $\Gamma > 0.002$) only extends about 5 μm ahead of the crack tip in Fig. 10b whereas the specimen width W is 300 μm so that small scale plasticity conditions prevail.

[1] Fatigue cannot occur in an elastic system because the state of the system then only depends on the current value of σ so that crack growth occurs in the first cycle or not at all.

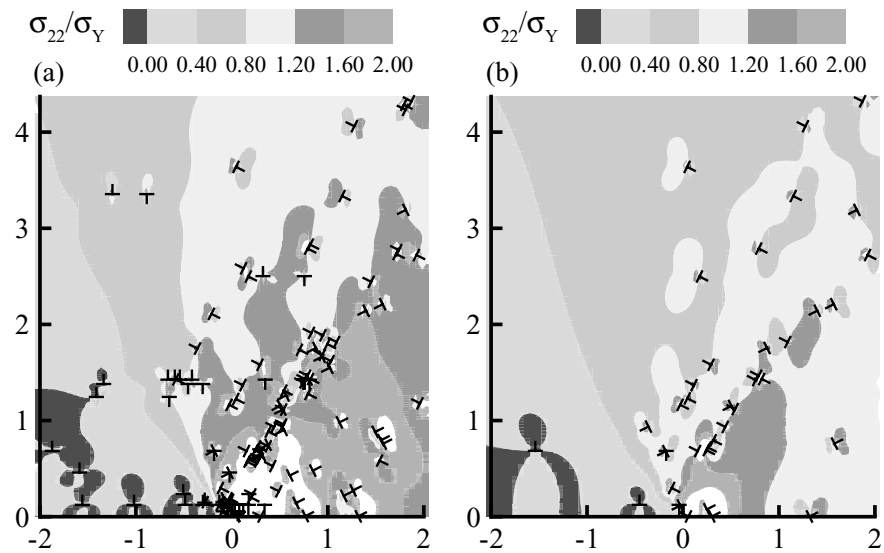

Fig. 9. Distribution of dislocations and opening stress σ_{22}/σ_Y in the neighborhood of the crack tip at the first load peak for the specimen with (a) a 10 μm edge crack with the near-threshold loading $\Delta\sigma_{th}/\sigma_Y \approx 0.4$ and (b) a 3 μm edge crack subject to $\Delta\sigma/\sigma_Y \approx 0.55$. The load ratio $R = 0.3$ in both cases. All distances are in μm.

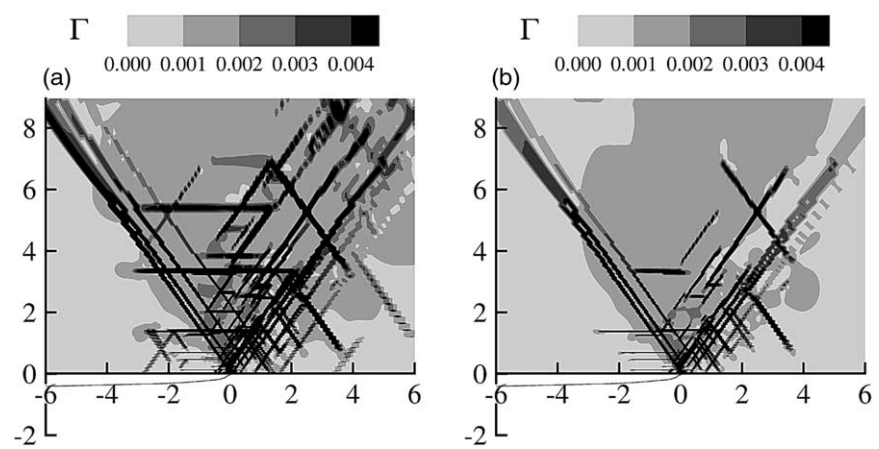

Fig. 10. (a) Contours of total slip $\Gamma = \sum|\gamma^{(\alpha)}|$ around the crack tip of the edge-cracked specimen with a=30 μm at a crack extension Δa=0.01 μm under (a) monotonic loading and (b) cyclic loading with the near-threshold loading $\Delta K_I/K_0$=0.603 (R=0.3). The crack opening profiles (displacements magnified by a factor of 20) are plotted below the x_1-axis. All distances are in μm.

5. Discussion

High cycle metal fatigue is generally observed to consist of a progression of events that ultimately lead to failure: surface crack nucleation, stage-I crack propagation, the transition to stage-II growth of the mechanically short crack and finally propagation of the long crack. Nucleation of surface cracks is considered to be connected with the build-up of local stresses and extruded material

where a persistent slip band (PSB) intersects the surface of the crystal (see [28] for recent developments and relevant references). These cracks then undergo stage-I crack growth along favorably orientated primary slip planes by "shear-decohesion" [5]. At some point the cracks transition to stage-II and become mechanically short mode-I cracks [29,30].

Our calculations correspond to mode-I, stage-II cracks. There is extensive experimental evidence for the anomalously high growth rate of mechanically short mode-I cracks for polycrystalline metals [4,11] and for single crystals [5,6]. By focusing on geometrically similar specimens, the effect of size is analyzed with the relation between the stress and stress intensity factor measures of the imposed loading fixed as given by Eq. (10). Consistent with the experimental observations, our calculations predict that the fatigue threshold ΔK_{th} decreases with decreasing crack length below a certain critical value of the crack length. Further, the model predicts that for $a < 100$ μm cyclic crack growth occurs with $K_{max} < K_0$. In contrast, under monotonic loading, the calculated K_{init} decreases only slightly with decreasing crack length due to the higher stresses associated with the denser near tip dislocation structures, but K_{init} remains greater than K_0 for all cases analyzed.

It is perhaps at first surprising that crack growth occurs under cyclic loading conditions even when K_{max} is less than K_0. What permits this is the net anti-shielding effect of the near tip dislocation structure that develops under cyclic loading conditions. By definition, (8), K_0 is a measure of the work of separation, ϕ_n, which must be supplied to the cohesive surface for crack growth to take place. Hence, at the crack tip, the "local K" regarded as a measure of the driving force for crack growth cannot be (and is not) less than K_0. On the other hand, K_{max} is a measure of the applied stress σ_{max} via (10) and there is no requirement that K_{max} reach K_0; the driving force for crack growth can substantially exceed K_{max}. Indeed, the occurrence of fatigue crack growth below the "Griffith limit" was noted in Ref. [26] and experimental measurements by Chan et al. [31] of the deformation field around the crack tip of cyclically loaded 7075 aluminum specimens indicated that the local crack tip driving force, as quantified through a cyclic crack field characterizing parameter, [32], was enhanced by a factor of two for the same applied ΔK for crack sizes less than 500 μm.

Values of $K_{max}/K_0 < 1$ are consistent with $\sigma_{max}/\sigma_Y < 1$ for small cracks. To illustrate this, neglect constants of order unity in Eqs. (8) and (10) and write the ratio K_{max}/K_0 as

$$\frac{K_{max}}{K_0} \approx \left(\frac{\sigma_{max}}{\sigma_Y}\right) \frac{\sqrt{a/\delta_n}}{\sqrt{E\sigma_{coh}/\sigma_Y^2}} = \sigma_{max} \frac{\sqrt{a/\delta_n}}{\sqrt{E\sigma_{coh}}}. \qquad (12)$$

For a 10 micron crack size, the calculations give a value of the fatigue threshold of $\sigma_{max}/\sigma_Y \approx 0.5$, Fig. 8, which is in the range of small crack fatigue limits observed experimentally, see e.g. Refs. [7,9,11]. With $E/\sigma_Y \approx 10^3$, $\sigma_{coh}/\sigma_Y \approx 10$, and $a/\delta_n \approx 10^4$, Eq. (12) implies $K_{max}/K_0 \approx \sigma_{max}/\sigma_Y < 1$. Note that, given σ_{max}, the value of K_{max}/K_0 in Eq. (12) is independent of the flow strength σ_Y. Also, K_{max}/K_0 in Eq. (12) only depends on σ_{coh} and δ_n through their product, and $\phi_n = \exp(1)\sigma_{coh}\delta_n$ is of the order of 1 J/m^2 for a wide range of materials.

All calculations in this investigation have been carried out with a/W=0.1. In Ref. [33] similar calculations were carried out for $a/W = 0.5$. The qualitative behavior is similar to that in the present calculations but, of course, there are quantitative differences. For example, the crack length at which deviation from the long crack limit occurs is at 100 μm rather than the 300 μm found here. A notable difference is that under monotonic loading, K_{init} is less than K_0 for $a = 5$ μm. However, with $a = 5$ μm and $a/W = 0.5$, plastic flow occurs over a size scale comparable to that of the ligament and small scale plasticity conditions are not met. In addition, fatigue crack growth is found with $a = 5$ μm, so that the minimum crack size for which mode-I fatigue crack growth is predicted depends on a/W.

Kitagawa and Takahashi [4] showed that the fatigue limit in a variety of ductile metals is characterized by a critical stress range $\Delta\sigma_{th}$ for sufficiently short cracks. The discrete dislocation results, Fig. 8b, show that fatigue is ΔK-governed for long cracks but the $\Delta\sigma_{th}$ versus a curve flattens out with decreasing crack length a and deviates

significantly from ΔK-governed fatigue, consistent with the experimental observations. Also consistent with experimental observations for short cracks, crack growth takes place with σ_{max} significantly less than the yield strength of the uncracked solid.

The overall behavior with crack size that comes out of our calculations is in accord with the identification of regimes in Vasudevan et al. [13], Figs. 13 and 14, and with a wide range of experimental observations including, for example, that short mode-I cracks remain sharp and grow under cyclic loading conditions while the same crack would blunt and arrest under monotonic loading conditions. The fatigue crack growth behavior of long cracks with contained plasticity is governed by the elastic stress intensity factor (ΔK_I and K_{max}). Below a critical crack size, crack growth is faster than what would be predicted by K-governed crack growth. However, for sufficiently small cracks factors not included in the present analysis, for example mixed mode loading, the internal stresses in persistent slip bands, [34], and internal stresses associated with a pre-existing dislocation structure likely play significant roles in promoting crack growth when it occurs.

Usami and Shida [9] postulated that the fatigue threshold corresponds to a critical size of the cyclic plastic zone for all crack sizes, but provided no physical basis for this hypothesis. Our discrete dislocation simulations reveal that stage-II fatigue crack growth occurs when the dislocation density (or the number of dislocations) in the vicinity of the crack tip reaches a critical value. An examination of the deformation fields around the crack tip at near-threshold values of applied ΔK_I reveals that slip is confined to approximately a V-shaped region emanating from the crack tip as seen in Fig. 10b. Defining the size of this plastic zone as the maximum vertical distance from the crack tip where $|\gamma^{(\alpha)}| \geq 0.004$ on all three slip systems $\alpha = 1, 2, 3$ in the sector $-35.3° \leq \phi \leq 35.3°$, the extent of the plastic zone was approximately 1.8 μm irrespective of crack length at the load peaks for near-threshold values of applied ΔK_I. Thus, our simulations provide a physical basis for the hypothesis in [9] (but the reason is because of near tip anti-shielding not because of plastic flow). In addition, the threshold value of crack tip opening displacement, $2u_2(x_1,0)$, at the load peak (taken as an average opening on the crack surface between 0.8 μm and 1.2 μm behind the crack tip) was ≈0.016 μm independent of crack length.

Experimental measurements by Breat et al. [35] of crack closure for short fatigue cracks in steel indicated that the differences between short and long cracks can be rationalized by accounting for crack closure, i.e. the effective stress intensity factor defined by $\Delta K^{eff} = K_{max} - K_{op}$, where K_{op} is the stress intensity at which the crack opens, uniquely defines the crack growth rate of both long and short cracks. However, this idea is not supported by other experimental studies. For example, measurements of crack closure by Ritchie and Yu [36] and Ritchie et al. [37] for aluminum alloys tested at a load ratio $R = 0.1$ show that crack closure effects alone cannot explain the faster crack growth rates of short cracks (readers are referred to [1] for discussion). In our simulations, where $R = 0.3$, complete crack closure does not occur and $\Delta K_{th} = \Delta K_{th}^{eff}$. Thus, the reduction in the fatigue threshold seen in Fig. 8a is solely due to *intrinsic* mechanisms in the classification scheme of Suresh and Ritchie [38] and in particular due to the evolution of the near tip stress and deformation state with continued cyclic loading. Indeed, the calculations here, as well as those in Refs. [14,15], quantify the role of internal stresses arising from an evolving dislocation structure in promoting fatigue crack growth.

Discrete dislocation plasticity coupled with a cohesive description of separation gives a coherent perspective on fracture in crystalline solids under both monotonic and cyclic loading conditions. The key to crack growth is the dual role played by dislocations: the dissipation associated with dislocation motion increases the resistance to crack growth, while the local stress concentration associated with discrete dislocations in the vicinity of the crack tip leads to stress levels of the magnitude of the cohesive strength, causing the crack to propagate. Under monotonic loading, as noted by Cleveringa et al. [18], two limiting cases can be identified. One, which is dislocation source limited, gives rise to brittle fracture. The other, which is

obstacle limited, leads to progressive blunting of the crack, with crack growth by decohesion being precluded. In this case, which is typical of ductile metals, fracture eventually occurs by void nucleation, growth and coalescence. There is a window, typically narrow, between these two limiting cases where crack growth by decohesion occurs in the presence of plasticity.

The behavior is quite different under cyclic loading conditions. The irreversibility of dislocation motion permits the number (or density) of dislocations in the near crack tip region to increase as cyclic loading proceeds. Because of the anti-shielding character of the near tip dislocation structure, crack growth can take place under cyclic loading conditions in circumstances where it is precluded under monotonic loading conditions. In our calculations, separation takes place through a mode-I cohesive surface constitutive relation which directly models decohesion with, for the parameter values employed, $\sigma_{coh}/\sigma_Y \approx 14$. However, our analyses also pertain when the actual process of crack growth is more complicated than direct mode-I separation provided that: (i) the overall mode of crack growth is mode-I on the length scale modeled; and (ii) the crack growth mechanism involves high local stresses. In this regard it is worth noting that the mechanism of fatigue crack growth is often viewed as taking place via dislocation emission from the crack tip, [39,40], and this mechanism requires high local stresses [41]. Indeed, the requirement of a high opening stress for crack growth underlies the enhanced growth rate of short cracks in our analyses. The stress enhancement from dislocation structures, which is what gives rise to the high stresses in the crack tip region, is not modeled by classical plasticity theory which only captures the dissipation aspect of plastic deformation.

6. Conclusions

We have carried out analyses of the growth of mode-I edge cracks under tensile loading conditions in geometrically similar single crystal specimens of varying size. The material is initially dislocation free, with dislocation nucleation occurring from Frank-Read sources distributed randomly in the material and with no special dislocation nucleation from the crack tip. The only difference between the analyses for monotonic and cyclic crack growth is in the specification of the applied loading.

- The reduction in the fatigue threshold when the crack length is smaller than a critical size is an outcome of the analyses. However, for a sufficiently small crack size, only a sparse dislocation structure is generated and crack growth does not occur.
- The large reduction in ΔK_{th} for short cracks is due to the progressive increase in internal stress under cyclic loading which is associated with the dislocation structure in the vicinity of the crack tip. In contrast, under monotonic loading for the same range of crack sizes K_{init} only decreases somewhat with crack size.
- The near crack tip dislocation density, the plastic zone size and the crack tip opening displacement at σ_{max} for near-threshold values of ΔK_I are approximately independent of crack size.
- Crack closure does not occur in the circumstances analyzed.
- Slip in the vicinity of a mode-I crack under cyclic loading is more localized than for the same crack under monotonic loading.
- The results here and in Refs. [14] and [15] show that the fatigue threshold, Paris law behavior, striations and the accelerated growth of short cracks emerge naturally from a unified framework where plastic flow arises from the motion of large numbers of discrete dislocations and the fracture properties are embedded in a cohesive surface constitutive relation.

Acknowledgements

Support from the AFOSR MURI at Brown University on *Virtual Testing and Design of Materials: A Multiscale Approach* (AFOSR Grant F49620-99-1-0272) is gratefully acknowledged. We are pleased to acknowledge Profs. R.O. Ritchie, S. Suresh and W .O. Soboyejo for insightful discussions during the course of this work. We are also grateful

to Dr. H. Riedel for bringing Ref. [32] to our attention.

References

[1] Suresh S, Ritchie RO. Int Metals Rev 1984;29:445.
[2] Ritchie RO, Peters JO. Mat Trans 2001;42:58.
[3] Suresh S. Fatigue of materials. Cambridge UK: Cambridge University Press, 1998.
[4] Kitagawa H, Takahashi S. Proc. of the 2nd Int. Conf on Mechanical Behavior of Materials, 1976, 627.
[5] Ma BT, Laird C. Acta Metall 1989;37:325.
[6] Zhang XP, Wang CH, Ye L, Mai YW. Fatig Fract Eng Mater Struct 2002;25:141.
[7] Tanaka K, Nakai Y, Yamashita M. Int J Fract 1981;17:519.
[8] Wang CH, Hutchinson JW. Int J Fract 2001;109:263.
[9] Usami S, Shida S. Fatig Eng Mater Struct 1979;1:471.
[10] Caracostas CA, Shodja HM, Weertman J. Mech Mat 1995;20:195.
[11] Usami S. Fatigue thresholds. In: Backlund J, Blom A, Beevers CJ, editors. 1982;1:205.
[12] Nguyen O, Repetto A, Ortiz M, Radovitzky RA. Int J Fract 2001;110:351.
[13] Vasudevan AK, Sadananda K, Glinka G. Int J Fatigue 2001;23:S39.
[14] Deshpande VS, Needleman A, Van der Giessen E. Acta Mat 2001;49:3189.
[15] Deshpande VS, Needleman A, Van der Giessen E. Acta Mat 2002;50:831.
[16] Cleveringa HHM, Van der Giessen E, Needleman A. Int J Plast 1999;15:837.
[17] Van der Giessen E, Needleman A. Modeling Simul Mater Sci Eng 1995;3:689.
[18] Cleveringa HHM, Van der Giessen E, Needleman A. Mech Phys Solids 2000;48:1133.
[19] Nicola L, Van der Giessen E, Needleman A. Mat Sci Engin A 2001;309-310:264.
[20] Kubin LP, Canova G, Condat M, Devincre B, Pontikis V, Bréchet Y. Solid State Phenomena 1992;23-24:455.
[21] Rose JH, Ferrante J, Smith JR. Phys Rev Lett 1981;47:675.
[22] Rice JR. J Appl Mech 1968;35:379.
[23] Do T, Splinter SJ, Chen C, McIntyre NS. Surf Sci 1997;387:192.
[24] Cleveringa HHM, Van der Giessen E, Needleman A. Mat Sci Eng A 2001;317:37.
[25] Tada H, Paris PC, Irwin GR. The Stress Analysis of Cracks Handbook. St. Louis: Paris Prod. Inc, 1985.
[26] Guiu F, Stevens RN. The behavior of short fatigue cracks. In: Miller KJ, de los Rios ER, editors. 1986;122.
[27] Juang R-R, Lee S. J Appl Phys 1986;59:3421.
[28] Repetto EA, Ortiz M. Acta Mat 1997;45:2577.
[29] Miller KJ. Mat Sci Tech 1993;9:453.
[30] McDowell DL. Int J Fract 1996;80:103.
[31] Chan KS, Lankford J, Davidson DL. J Eng Mater Tech 1986;108:206.
[32] Wilthrich C. Int. J Fract 1982;20:R35.
[33] Deshpande VS, Van der Giessen E, Needleman A. Proc. 8th Int Fatig Congress. In: Blom AF, editor. 2002;2:1397.
[34] Brown LM. Ashby Symposium: The modeling of material behavior and design. In: Embury JD, Thompson AW, editors. 1990;178.
[35] Breat JL, Mudry F, Pineau A. Fatig Eng Mat Struct 1983;6:349.
[36] Ritchie RO, Yu W. Small Fatigue Cracks. In: Ritchie RO, Lankford J, editors. 1986;167.
[37] Ritchie RO, Yu W, Blom AF, Holm DK. Fatig Fract Eng Mater Struct 1987;10:343.
[38] Suresh S, Ritchie RO. Met Trans 1981;13A:397.
[39] Laird C, Smith GC. Phil. Mag 1962;7:47.
[40] Neumann P. Acta Metall 1969;17:1219.
[41] Beltz GE, Rice JR. Acta Metall 1992;40:321.